TWENTY FIRST EUROPEAN ROTORCRAFT FORUM

Paper No. II - 6

CALCULATIONS OF MULTIBLADED ROTORS IN HOVER USING 3D EULER METHODS OF DLR AND ONERA

J. Raddatz

DLR, Institute of Design Aerodynamics
Germany

O. Rouzaud

ONERA, Aerodynamics Division
France

August 30 - September 1, 1995
Saint Petersburg
Russia

Paper nr.: II.6

Calculations of Multibladed Rotors in Hover Using 3D Euler Methods of DLR and ONERA.

J. Raddatz; O. Rouzaud

TWENTY FIRST EUROPEAN ROTORCRAFT FORUM
August 30 - September 1, 1995 Saint-Petersburg, Russia

TWENTY FIRST EUROPEAN ROTORCRAFT FORUM

Paper No. II - 6

CALCULATIONS OF MULTIBLADED ROTORS IN HOVER USING 3D EULER METHODS OF DLR AND ONERA

(Presentation of Results obtained within EU Project HELISHAPE)

J. Raddatz

DLR, Institute of Design Aerodynamics
Lilienthalplatz 7, 38108 Braunschweig, Germany

O. Rouzaud

ONERA, Aerodynamics Division
BP 72, 92322 Châtillon Cedex, France

Summary:

Two different Euler codes for hovering rotor calculations, developed by DLR and ONERA, are compared and assessed using common computational grids. The test cases are based on the Caradonna-Tung data base and on the new HELISHAPE tests with 4-bladed 7A rotor, scheduled for end of 1995.

For all test cases the predicted pressure distributions of both codes are in good agreement. Considering that Euler calculation do not account for viscous effects the predicted surface data also compare well with experiments.

A detailed comparison of the wake and tip vortex representation by both Euler methods shows some differences. The strong effects of numerical diffusion on wake resolution are demonstrated. It is found that a detailed wake and vortex representation hinders the convergence to steady state of the Euler methods, particularly the integrated flow quantities oscillate with iteration in a low-frequency limit cycle.

Both Euler methods provide encouraging results concerning surface data without relying on any wake model. The detailed examination of the rotational flow phenomena of an hovering rotor is a difficult subject that requires future research.

Symbols:

c	chord
c_p	pressure coefficient $c_p = \dfrac{p - p_\infty}{\frac{1}{2}\rho_\infty (\omega \cdot r)^2}$
C_T	thrust coefficient
E	total specific energy
$\overline{\overline{F}}$	flux tensor
$\vec{G}$	vector of source terms
H	total specific enthalpy
M	Mach number
$\vec{n}$	unit outward to ∂V
p	pressure
$\vec{q}$	velocity vector
r	radial position of a rotor section
$\vec{r}$	$= (x, y, z)^T$ coordinate vector
R	rotor radius
dS	surface element
t	time
u, v, w	Cartesian velocity components
V	control volume
dV	volume element
$\vec{W}$	vector of conservative variables
x, y, z	Cartesian coordinates
γ	ratio of specific heats
θ	pitching angle
ρ	density
σ	solidity of the rotor
ψ	azimuth
ω	angular velocity
Index r	blade fixed coordinate system

1. Introduction

Numerical simulation of the flowfield of a helicopter is a challenging problem. The complexity of the flow stems from several peculiar features that are unique to a helicopter. Much of the flow in the vicinity of the rotating blades is nonlinear, three dimensional and often unsteady. In addition, the blades shed complex vortical wakes. The presence of the vortical wake and its interaction with the blades affects the performance, blade loads, vibrations and acoustics of a helicopter. Accurate prediction of the rotor wake system is one of the most difficult problems in rotorcraft aerodynamics. Since the rotor and its wake constitute a tightly coupled system it is natural to solve the flow around the blade and the wake with a unified flow method.

Within the EU project HELISHAPE solutions of the Euler equations are used to predict the flow of an isolated rotor in hover. Euler equations describe the complete inviscid flowfield of a rotor including the wake and its induced effects, provided that the grid contains the whole rotor disk. Since the flow around an hovering rotor can be treated as steady, the complexity of the flow field is considerably reduced. On the other hand, the vortical wake and the mutual blade-vortex interactions are major features of the hovering rotor aerodynamics. Therefore the hover case is an appropriate test case for improvements of CFD codes for rotor flows and investigations concerning the accuracy of the predicted rotational flow phenomena.

The theoretical results are produced using the existing Euler codes of DLR and ONERA for multibladed rotor applications. All calculations are performed on common grids. This allows a direct comparison of the codes and provides a detailed elaboration of the capabilities and limits of the different numerical strategies. Since both codes are based on different theoretical approaches, critical components of the integration schemes (e.g. space discretization, treatment of boundary conditions, time integration) can be assessed with respect to efficient and accurate unified blade/wake calculations for realistic rotors.

In order to check the reliability of the Euler codes for a wide range of applications several test cases have been selected. For one test case a grid convergence study is carried out to check the accuracy of the methods. The test cases include the well documented Caradonna-Tung data base as well as the new HELISHAPE tests using a 4-bladed rotor with different tip shapes. Compared to the simple geometry of the Caradonna-Tung rotor, the 4-bladed HELISHAPE rotors represent scaled versions of realistic multibladed rotors as they are used for modern helicopters. The paper presents and compares only pre-test calculations for the HELISHAPE rotor with rectangular tip shape, performed by the different Euler methods. As the HELISHAPE wind tunnel tests are scheduled for end of 1995, comparisons with experimental data are not possible yet.

In addition to the comparisons of results on the blade surface, the investigations presented in this paper are directed towards the accurate modelling of the complete hover flowfield. Using flow field visualization tools the wake geometry, especially the trajectories and shape of the calculated tip vortices are shown.

2. Governing Equations

Both Euler methods for hovering rotors, used within this paper, solve the 3D compressible Euler equations transformed in a blade attached rotating reference frame. In this reference frame the Euler equations are formulated in terms of absolute velocities, which is necessary for an accurate formulation of the farfield boundary condition.

The Euler equations in Cartesian coordinates are written in integral form as:

$$\frac{d}{dt}\int_{V_r} \vec{W}_r \, dV_r + \int_{\partial V_r} \bar{\bar{F}}_r \cdot \vec{n}_r \, dS_r + \int_{V_r} \vec{G}_r \, dV_r = 0$$

$\vec{W}_r$ represents the conserved vector of absolute flow variables, $\bar{\bar{F}}_r$ the corresponding flux tensor and $\vec{G}_r$ is a source term.

For an hovering rotor rotating around the x-axis with the angular velocity $\vec{\omega} = [\Omega, 0, 0]^T$ these quantities are given by:

$$\vec{W}_r = \begin{bmatrix} \rho \\ \rho u_r \\ \rho v_r \\ \rho w_r \\ \rho E_r \end{bmatrix}, \qquad \vec{G}_r = \begin{bmatrix} 0 \\ 0 \\ -\rho \Omega w_r \\ \rho \Omega v_r \\ 0 \end{bmatrix},$$

$$\bar{\bar{F}}_r = \begin{bmatrix} \rho\,[\vec{q}_r - (\vec{\omega}\times\vec{r}_r)\,] \\ \rho u_r\,[\vec{q}_r - (\vec{\omega}\times\vec{r}_r)\,] + p\vec{i}_{x_r} \\ \rho v_r\,[\vec{q}_r - (\vec{\omega}\times\vec{r}_r)\,] + p\vec{i}_{y_r} \\ \rho w_r\,[\vec{q}_r - (\vec{\omega}\times\vec{r}_r)\,] + p\vec{i}_{z_r} \\ \rho H_r\,[\vec{q}_r - (\vec{\omega}\times\vec{r}_r)\,] \end{bmatrix}$$

The relative velocity $\vec{q}_r$ is given by:

$$\vec{q}_r = \begin{bmatrix} u_r \\ v_r \\ w_r \end{bmatrix} = \begin{bmatrix} 1 & 0 & 0 \\ 0 & \cos\Omega t & \sin\Omega t \\ 0 & -\sin\Omega t & \cos\Omega t \end{bmatrix} \cdot \begin{bmatrix} u \\ v \\ w \end{bmatrix}$$

In the ONERA code the system of equations is closed by:

$$p = (\gamma - 1)\,\rho\left(E_r - \frac{\vec{q}_r^{\,2}}{2}\right)$$

and $H_r = E_r + p/\rho$.

For the DLR method the governing equations described above are slightly modified. For details see Ref. [1]. Within the energy equation the variables E_r and H_r are replaced by $\tilde{E}_r$ and $\tilde{H}_r$

with $\tilde{E}_r = E_r - \vec{q}_r\,(\vec{\omega}\times\vec{r}_r)$

and $\tilde{H}_r = H_r - \vec{q}_r\,(\vec{\omega}\times\vec{r}_r)$.

The system of equations used by the DLR method is closed by:

$$p = (\gamma - 1)\,\rho\left(\tilde{E}_r - \frac{\vec{q}_r^{\,2} - 2\vec{q}_r\cdot\vec{\omega}\times\vec{r}_r}{2}\right)$$

and $\tilde{H}_r = \tilde{E}_r + p/\rho$.

$\tilde{H}_r$ is the so called rothalpy, which is constant in the whole flow field for the case of an adiabatic steady flow in the rotating coordinate system. These modified governing equations with rothalpy $\tilde{H}_r$ instead of H_r provide the advantage of using rothalpy damping as an additional acceleration technique.

3. DLR Euler Method for Hovering Rotors

3.1 Spatial and Temporal Discretization

The discretization of space and time is separated following the method of lines (Jameson et al. [2]) using a cell-vertex finite volume formulation for the spatial discretization. The flow quantities are located at the nodes of the grid. The finite volume discretization with central differencing for the flux approximation leads to a 2. order scheme on a Cartesian grid with constant grid spacing. If an arbitrary nonuniform grid is used, the accuracy depends on the smoothness of the grid. For the cell-vertex scheme a minimum of 1. order accuracy is guaranteed for arbitrary grids (for details see Ref. [3]). In order to avoid spurious oscillations a blend of first and third order dissipative terms is introduced.

An explicit 5-stage Runge-Kutta time stepping scheme is used with an evaluation of the dissipative fluxes only at the first two stages [4]. In order to accelerate the convergence to steady state for hover cases, rothalpy damping, implicit residual averaging and a multigrid algorithm have been implemented.

3.2 Boundary Conditions

For the blades a solid wall condition is used at the surface. This boundary condition zeroes the normal component of the velocity vectors at the surface nodes of the body fitted grid and ensures flow parallel to the wall. The farfield boundaries are treated following the concept of characteristic variables for non-reflecting boundary conditions. At the inboard plane boundary near the axis of rotation the DLR code uses a solid wall condition. Finally, the treatment of all cut boundaries including the periodicity boundaries involves two layers of ghost cells obtaining 2. order accuracy at these boundaries.

4. ONERA Euler Method for Hovering Rotors

4.1 Spatial and Temporal Discretization

A detailed description of the ONERA Euler method for hovering rotors is given in Ref. [5] and [6]. The Euler equations in integral form are discretized on a curvilinear structured grid using a cell-centered finite-volume approach.

The basic implicit Euler solver is implemented by means of two successive stages at each time step:

- an explicit stage of second order of accuracy which is an original multidimensional version of the Lax-Wendroff scheme, fourth order linearly dissipative, involving one predictor in each space direction [7],
- an implicit stage of the order of the truncation error of the global scheme allowing the use of high CFL numbers [8].

Up to now, for three dimensional applications, the implicit stage is split into each space-direction using the ADI factorization method, and simplified by replacing the block matrices by their spectral radii (Scalar Approximate Factorization) [9]. This leads to solving only simple well conditioned algebraic tridiagonal linear systems in each spatial direction. This simplification reduces the computational costs of the numerical simulation considerably. However, the CFL number is restricted to rather low values when using SAF to solve the implicit stage.
In this original space-centered method the intrinsic dissipation is due to the second order term of the explicit stage and increases with the CFL number. The method works without artificial viscosity in the transonic regime and the CFL number allowed by SAF is generally large enough to ensure Euler solutions with low dissipative errors and sharp numerical shock waves.

4.2 Boundary Conditions

On the blade surface, the slip condition is prescribed and the pressure is obtained from the discrete form of momentum equations in order to achieve a conservative approximation of the normal momentum equations. For farfield and hub boundaries, a unified computational procedure for the boundary fluxes has been recently developed following the concept of characteristic variables. It has been stated that the source term may influence wave propagation and therefore it is included in this approach.

5. Grid Generation

The grids for the test cases investigated in this paper have been generated by DLR. A grid generator based on an elliptic 3D solver (for details see [10]) has been used. Due to the cylindrical nature of the flow of an hovering rotor an O-H topology was chosen with the wraparound O-structure in chordwise direction and the H-type in spanwise direction. This grid topology is suitable for 2-bladed as well as for multibladed rotors (see Ref. [11]). The grid is clustered near the leading and trailing edges and near the tip region to resolve the tip vortex.
Due to the symmetry of the flow only a segment of the rotor plane containing one blade has to be regarded. The other blades are taken into account by periodicity conditions in the blade azimuthal direction, which swap the flow information at the front and back boundaries of the cylindrical mesh. Using this grid topology, it is obvious to generate grids with identical point distributions on the periodicity planes. Therefore, no interpolation of the flow quantities on the periodicity planes is required.

Fig. 1 presents the surface grid and two surrounding O-planes of the 2-bladed model rotor used by Caradonna and Tung. The complete grid shape is shown in Fig. 2. For a grid refinement study grids of three different sizes were generated starting with a coarse grid of 56 cells in the wraparound "O", 20 cells in the normal and 32 cells in the radial direction. The grid was refined two times in all three index directions obtaining a fine grid of about 2.3 million cells. Fig. 3 demonstrates the different grid sizes presenting the grid lines in the rotor disk.

The geometry of the 4-bladed HELISHAPE rotor with rectangular tip shape is shown in Fig. 4 and 5, presenting grid lines in the complete rotor disk (4 blades) and around one rotor blade. The size of the grid for the HELISHAPE rotor correspond to the medium grid of Caradonna-Tung rotor. Due to the higher aspect ratio of this rotor some cells in radial and normal direction are added, obtaining a grid of about 400 000 cells.

6. Results

Three test cases have been specified for validation and assessment of the DLR and ONERA Euler codes. The test cases include the well documented Caradonna-Tung data base [12] as well as new tests, which will be conducted within the EU project HELISHAPE:

Test case 1: Caradonna-Tung rotor:
The experimental model consists of a 2-bladed rigid rotor with untwisted, untapered, rectangular blades made of NACA 0012 airfoil sections with an aspect ratio of 6.
Test conditions:
$M_{\omega R} = 0.794$, $\theta_{0.7} = 8.0°$
For this test case a grid refinement study is performed.

Test case 2: Caradonna-Tung rotor:

Test conditions:

$M_{\omega R} = 0.610, \theta_{0.7} = 12.0°.$

This test case includes an investigation concerning the prediction of the global flow phenomena of an hovering rotor like geometry of wake and tip vortices.

Test case 3: 4-bladed 7A rotor with rectangular planform shape (HELISHAPE test):
The 4-bladed HELISHAPE test rotor uses rigid, twisted blades with an aspect ratio of 15 and is made of OA2xx airfoils with varying thickness from 13 to 9 percent.

Test conditions:

$M_{\omega R} = 0.647, \theta_{0.7} = 7.5°.$

6.1 Comparison of Blade Surface Data for Test Cases 1and 2

Fig. 6-8 show predicted and experimental pressure coefficients at five different blade sections for test case 1. Fig. 6 and 7 compare, separately for ONERA and DLR, experimental data with the solutions conducted on the three grids with different grid sizes. The numerical results of DLR and ONERA show the typical behaviour of a grid refinement study with very small discrepancies between fine and medium grid solutions and some larger differences in the pressure values between medium and coarse grid solutions. These results indicate that the fine grid solutions are grid converged. In both figures, calculated shock positions obtained on the different grid sizes are identical. Larger discrepancies can be recognized in the prediction of the shock wave strength. In comparison with the DLR method, the ONERA Euler code show a somewhat sharper shock resolution, especially on the coarse grid.

A direct comparison of DLR and ONERA results is given in Fig. 8. There the pressure distributions obtained on the fine grid are shown. Overall both Euler calculations are in very good agreement. Small differences occur in the shock region resulting in a slightly different shock position.
On fine and medium grids both computations show an overprediction of the shock compared to the measured data. One reason is that the current calculations are inviscid. Shock/boundary layer interactions tend to weaken the shock. An inviscid method cannot model this phenomenon, so some discrepancies in predicted and measured shock strength and position are expected. Overall the Euler calculations are in good agreement with the experimental results on all radial stations.

Spanwise lift coefficients are plotted in Fig. 9 comparing medium and fine grid calculations of DLR and ONERA. Additionally, lift data determined from the measured pressure coefficients are given. The discrepancies between the computed lift coefficients are consistent with the computed surface pressure results. The effect of a different boundary treatment on the hub boundary in both Euler codes is obvious. Since Euler results are inviscid, an overprediction of the lift is expected. The poor agreement between computed and experimental lift data is mainly caused by the fact that the integration of experimental lift coefficients using only few measured pressure data is of low accuracy.

The comparison for blade surface data of test case 2 is presented in Fig. 10 and 11 showing pressure distributions at five sections and spanwise blade loadings. The lower tip speed for this test case produces only a weak shock on the blade. Therefore, the overall agreement between DLR and ONERA calculation is slightly better compared to the medium grid solutions of test case 1. Considering that Euler calculations are inviscid, the comparison with experimental pressure data shows also a good agreement.

Relative Mach numbers on the upper blade surface and the rotor disk are presented in Fig. 12 and 13 for both Caradonna-Tung test cases. The figures show differences at the blade tip and the rotor hub, probably caused by the different numerical treatment of spatial discretization, hub boundary and blade tip in the Euler codes of DLR and ONERA.

6.2 Comparison of Convergence Behaviour

Fig. 14 and 15 present convergence histories for DLR and ONERA calculations. Fig. 14 shows the convergence behaviour of the medium grid calculations of test case1. Three different calculations are shown: ONERA calculation, DLR multigrid and DLR singlegrid calculation. The figure demonstrates the great advantage of the DLR multigrid acceleration techniques, which reduces the number time steps considerably. Plotting the thrust coefficient after each time step (only DLR data available) proves

that the DLR multigrid solution is fully time converged. However, computing the hover test cases the DLR multigrid method needs high values of artificial dissipation for convergence. To improve accuracy of the DLR results, a second calculation has been performed using a low value for artificial dissipation in single grid mode. Results of low dissipative DLR computations are used for the comparisons of surface data in figures 6 - 13. The corresponding convergence history is also plotted in Fig. 14. The convergence behaviour looks quite similar to the ONERA calculation. The convergence history of the thrust coefficient of the low dissipative DLR solution indicates that the iteration process does not completely converge to steady state values, but oscillates with iteration in a low-frequency limit cycle.

The convergence behaviour for the high lift Caradonna-Tung test case (case 2) is shown in Fig. 15. Similar to the first case we have a fast, fully time converged solution for the DLR multigrid method, while the ONERA code and the DLR code in singlegrid mode show difficulties in convergence. Compared to test case 1 the oscillations in thrust coefficient have been increased. A similar convergence behaviour for hover calculations has also been shown with the TURNS Navier-Stokes code of Srinivasan, Baeder et. al. [14].

It is believed that the oscillations in thrust of the low dissipative DLR solutions (and probably the ONERA solutions) are caused by movement of the tip vortex. Using a coarser mesh, turning off the periodic blade-to-blade boundary conditions or diffusing the vortex using high artificial dissipation causes the oscillations to disappear. This statement corresponds to results of the Navier-Stokes code TURNS, presented in Ref. [14]. Further confirmation is given by F.X. Caradonna in Ref. [15]: "*It can be difficult to obtain a stable wake solution with any hover prediction method, because the wake is, in fact, inherently unsteady*". With regard to these statements it is questionable if a detailed representation of the rotor wake is possible using a steady prediction method.

6.3 Effects of Different Numerical Dissipation on Surface Data

In Fig. 16-18 results of two DLR calculations of test case 2 are compared, using different values of artificial dissipation. Test case 2 has been selected, because convergence histories of the thrust coefficient indicate larger differences for this hover case. Nevertheless, the differences in pressure, presented in Fig. 16 at three blade sections, are very small. Looking at the spanwise blade loadings in Fig. 17, small qualitative differences are found. They indicate a different prediction of location and strength of the tip vortex and the wake.

The comparison of relative mach number (Fig. 18) shows small differences in the tip region. Concerning the low dissipative solution the introduced dissipative terms are too small for smoothing the spurious high frequency oscillations near the tip. This is indicated by the lift coefficient and the shape of the iso-Mach lines.

6.4 Comparison of the Prediction of Flow Field Data like Wake and Vortices

A complete validation and assessment of the Euler codes of DLR and ONERA includes the investigation of the prediction of rotational phenomena in the flow field like the wake or the tip vortex. Investigations concerning the effect of grid refinement (test case 1) on the representation of the wake system of an hovering rotor have already been published in [13]. Therefore, the comparison of the flowfield prediction capabilities of both codes will be presented only for test case 2.

The flow field investigations are performed by extracting 2D radial slices, which are located nearly perpendicular to the mean flow direction. Plotting vorticity contours (magnitude of the local rotation vectors $= |\vec{V} \times \vec{q}|$) the 2D slices show a good representation of the wake and the tip vortices.
The radial location of the slices presented in this paper are indicated in Fig. 19. The figure shows the grid lines in the rotor disk and the five different radial slice positions at 20°, 40°, 70°, 100° and 140° behind the blade.

The vorticity contours of all 2D slices are presented in Fig. 20. There are three plots for each 2D slice: DLR multigrid solution (high dissipation) on the left side, DLR singlegrid solution (low dissipation) and ONERA solution on the right side. Comparing the different DLR solutions the influence of a high artificial dissipation producing a high numerical diffusion is obvious. With high dissipation the computed tip vortex is resolved less sharply and the diffusion by time runs faster. Additionally there are small differences in the predicted position of the vortex.

Although the low dissipation DLR solution and the ONERA solution show a very similar convergence behaviour there are remarkable discrepancies. While the DLR code predicts the tip vortex for a longer distance the ONERA method shows a better resolution of the wake.

Quantitative measurements of the vortex trajectories are compared with predicted values in Fig. 21. A dashed line represents the experimental data from Ref. [12]. The computed vortex trajectories were obtained using the results from Fig. 20 to locate the centers of vortices graphically. The coordinate values of these vortex centers are obtained at discrete azimuthal angles and then transferred to the plots in Fig. 21. The predicted radial contraction of the tip vortex shows reasonable agreement to the experimental data up to a vortex age of 250°. The best agreement was found for results of the low dissipation DLR calculation. The large discrepancies between measurement and prediction for a vortex age above 250° is caused by an insufficient grid resolution, which prevents a separated vortex representation.
The vertical descent of tip vortex is predicted qualitatively correct by both DLR calculations up to a vortex age of 250°. Although the ONERA calculations exhibit closer agreement to the experimental data in terms of magnitude, the DLR calculations, with an obvious offset, better match the slope of the experimental data curve. As presented in Ref. [13] a refinement of the grid resolution improves the predictions of vertical descent considerably.

6.5 Comparison of Blade Surface Data for Test Case 3

Results of pre-test calculations for the 4-bladed HELISHAPE 7A rotor are presented in Fig. 22 and 23. Fig. 22 shows predicted pressure coefficients at five different blade sections, Fig. 23 spanwise blade loadings. Concerning pressure distributions the agreement of the Euler predictions of DLR and ONERA is good. The predicted blade loadings show differences near the hub $(r/R < 0.5)$ and over the outer span of the blades $(0.8 < r/R < 0.9)$. The variation in lift coefficient near the hub is caused by the different hub boundary treatment. It is believed that the differences in the predicted loadings over the outer span result from differences in the prediction of tip vortex position and strength. For detailed investigations of these effects and to improve the accuracy of loading prediction accurate measurements of thrust, sectional lift coefficients and location and strength of the tip vortex, performed on rigid rotor blades, are required.

7. Conclusion

Under a cooperative EU program the Euler codes for hovering rotors, developed by DLR and ONERA, are being compared and assessed using common computational grids.

Concerning the surface data on the rotor blades the results of both Euler codes show a good agreement for all test cases. Through a grid refinement study, it was demonstrated that the small differences in the calculated surface data are reduced if the discretization errors are decreased using finer grids. Keeping in mind that Euler calculations do not account for viscous effects, the surface data predicted on the medium grid show already a good agreement with the experimental data. Even coarse grid calculations may be acceptable for engineering purposes, as long as only flow quantities on the blade surface are of interest.

The advantage of the ONERA method is the slightly better shock resolution, especially for calculations on a coarse mesh. A comparison of the convergence behaviour shows the advantage of the DLR code, which has a clearly better convergence to steady state if the multigrid algorithm is used. Although the multigrid technique needs larger values of artificial dissipation there are only small effects on the calculated surface results. Further improvements of both Euler methods are on the way. ONERA will introduce an efficient relaxation method [16] to increase the convergence speed. Shock resolution of the DLR code shall be improved using a cell-vertex upwind scheme [17].

A comparison concerning the accurate modelling of the complete flowfield of an hovering rotor has been performed for the high lift Caradonna-Tung test case. Investigations concerning the influence of artificial dissipation demonstrates the strong effects of numerical diffusion on the wake and vortex resolution. Both Euler methods do not accurately resolve the wake of an hovering rotor for a large enough distance using an affordable number of grid points. Higher-order differencing methods, radically finer grids, or other meshing strategies like Chimera grid embedding or adaptive gridding, may help to resolve this problem. On the other hand, a good

wake and vortex resolution seems to hinder the iterative process to converge to a steady state solution. Of course, further research is needed to get a better understanding of the unsteadiness of the hovering rotor wake and the effects of wake resolution on the convergence behaviour of Euler or Navier-Stokes methods.

In conclusion both Euler methods are providing encouraging results concerning surface data without relying on additional wake models. The detailed examination of the flow phenomena in hover requires further enhancements to methods and grid generation. With regard to Ref. [14] an accurate prediction of tip-vortex position and strength is finally needed for predicting the hovering performance using a Navier-Stokes method.

8. Acknowledgements

This work, which is part of the HELISHAPE project, is funded by the European Union under the BRITE/ EURAM programme. Development of ONERA Euler method was funded by French Ministry of Defence (DRET).
The authors would like to thank N. Kroll an J. Sidès for their encouragement and useful discussions. The second author would also like to thank J.C. Boniface for his assistance with the use of the ONERA Euler code.

9. Bibliography

[1] Kroll, N.: *'Computation of the Flow Fields of Propellers and Hovering Rotors using Euler Equations'*, 12th European Rotorcraft Forum, Paper 28, Garmisch-Partenkirchen, Germany, Sep. 1986.

[2] Jameson, A.; Schmidt, W.; Turkel, E.: *'Numerical Solutions of the Euler Equations by Finite Volume Methods Using Runge-Kutta Time Stepping Schemes'*, AIAA-Paper 81-1259 (1981).

[3] Rossow, C.-C.: *'Berechnung von Strömungsfeldern durch die Lösung der Euler-Gleichungen mit einer erweiterten Finite-Volumen Diskretisierungsmethode'*, DLR-FB 89-38, Braunschweig,1989.

[4] Kroll, N. and Jain, R. K.: *'Solution of Two-Dimensional Euler Equations - Experience with a Finite Volume Code'*, DFVLR-FB 87-41, Braunschweig, 1987.

[5] Boniface, J.C. and Sidès, J.: *'Numerical Simulation of Steady and Unsteady Euler Flows around Multibladed Helicopter Rotors'*, 19th European Rotorcraft Forum, Paper C10, Cernobbio (Como), Italy, Sep. 1993.

[6] Boniface, J.C. and Sidès, J.: *'Extension and Improvement of existing Euler Code of ONERA for multibladed Rotors in Hover'*, HELISHAPE Technical Report, 1995.

[7] Lerat, A.: *'Sur le calcul des solutions faibles des systèmes hyperboliques de lois de conservation à l'aide de schémas aux différences'*, ONERA Publication No. 1981-1, 1981.

[8] Lerat, A.: *'Implicit Methods of Second-Order Accuracy for the Euler Equations'*, AIAA Paper No. 83-1925 and AIAA Journal Vol. 23, pp. 33-40, 1985.

[9] Lerat, A., Sidès, J. and Daru, V.: *'An Implicit Finite-Volume Method for Solving the Euler Equations'*, Lecture Notes in Physics, Vol. 17, pp. 343-349, Springer Verlag Ed., 1982.

[10] Findling, A. and Herrmann, U.: *'Development of an efficient and robust solver for elliptic grid generation'*, Proceedings of the Third International Conference on Numerical Grid Generation in Computational Fluid Dynamics and Related Fields, Barcelona, Spain, 1991.

[11] Pahlke, K. and Raddatz, J.: *"3D Euler Methods for Multibladed Rotors in Hover and Forward Flight'*, 19th European Rotorcraft Forum, Paper C20, Cernobbio (Como), Italy, Sep. 1993.

[12] Caradonna, F. X. and Tung, C.: *'Experimental and Analytical Studies of a Model Helicopter Rotor in Hover'*, NASA TM-81232, Sep. 1981.

[13] Raddatz, J. and Pahlke, K.: *"3D Euler Calculations of Multibladed Rotors in Hover: Investigations of the Wake Capturing Properties'*, 75th AGARD Fluid Dynamics Panel Symposium on 'Aerodynamics and Aeroacoustics of Rotorcraft', Berlin, Germany, Oct. 1994.

[14] Wake, B.E. and Baeder, J.D.: *'Evaluation of the TURNS Analysis for Hover Performance Prediction'*, American Helicopter Society Aeromechanics Specialists Conference, San Francisco, Jan. 1994.

[15] Caradonna, F.X.: *'Recent Methods for the Prediction of Rotor-Wake Problems'*, Lecture held at the Int. Colloquium VORTEX FLOWS IN AERONAUTICS, Aachen, Germany, Oct. 1994.

[16] Corre, C., Khalfallah, K. and Lerat, A.: *'An efficient relaxation method for a 3D centered Euler Solver'*, Proceed. 5th Inter. Symp. on Computational Fluid Dynamics, Sendai, Japan, Vol. 1, pp. 122-129, 1993.

[17] Rossow, C.C.: *'Accurate Solution of the 2-D Euler Equations with an Efficient Cell-Vertex Upwind Scheme'*, AIAA Paper No. 93-0071, 1993.

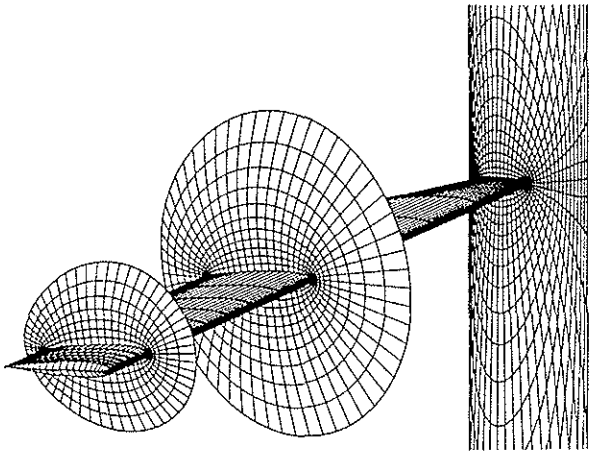

Figure 1 : Surface grid and surrounding O-type planes of Caradonna-Tung rotor

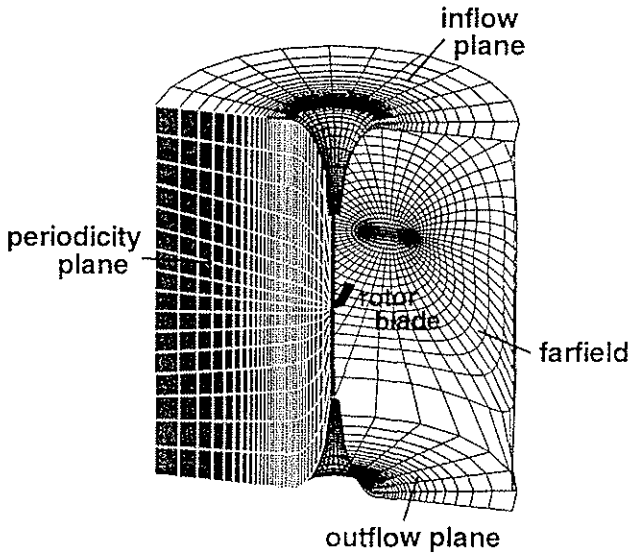

Figure 2 : O-H grid around one blade of 2-bladed Caradonna-Tung rotor

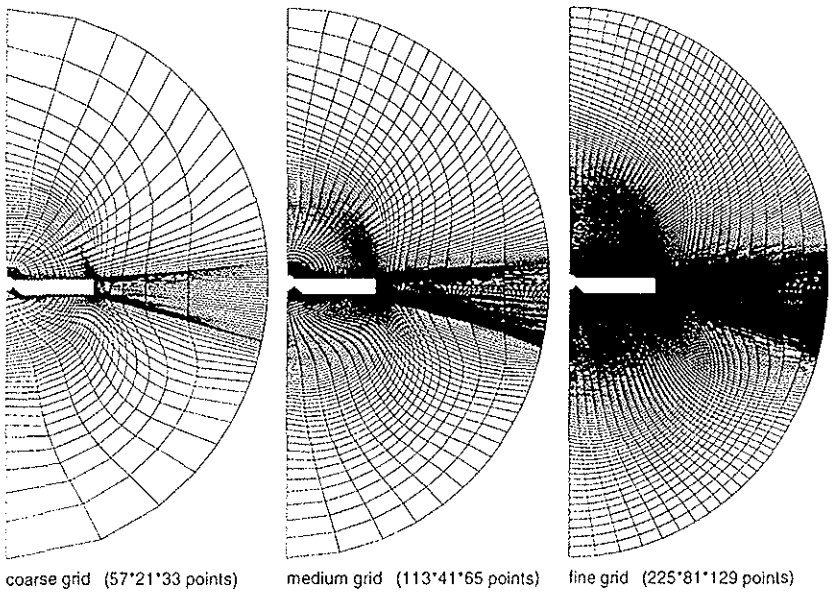

Figure 3 : Grid refinement study: Grid lines in the rotor disk of Caradonna-Tung rotor

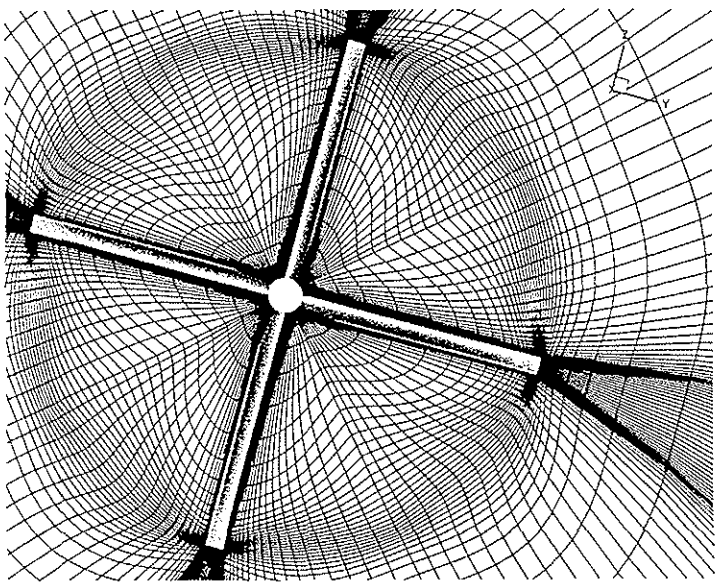

Figure 4 :

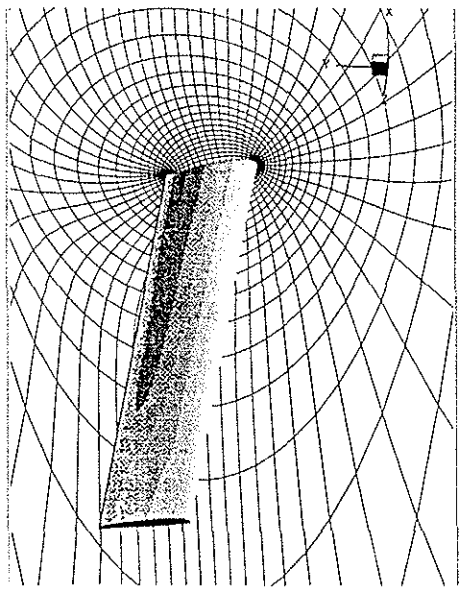

Figure 5 :

Grid lines in the rotor disk and around the rotor blade for HELISHAPE rotor 7A (every 2nd line drawn)

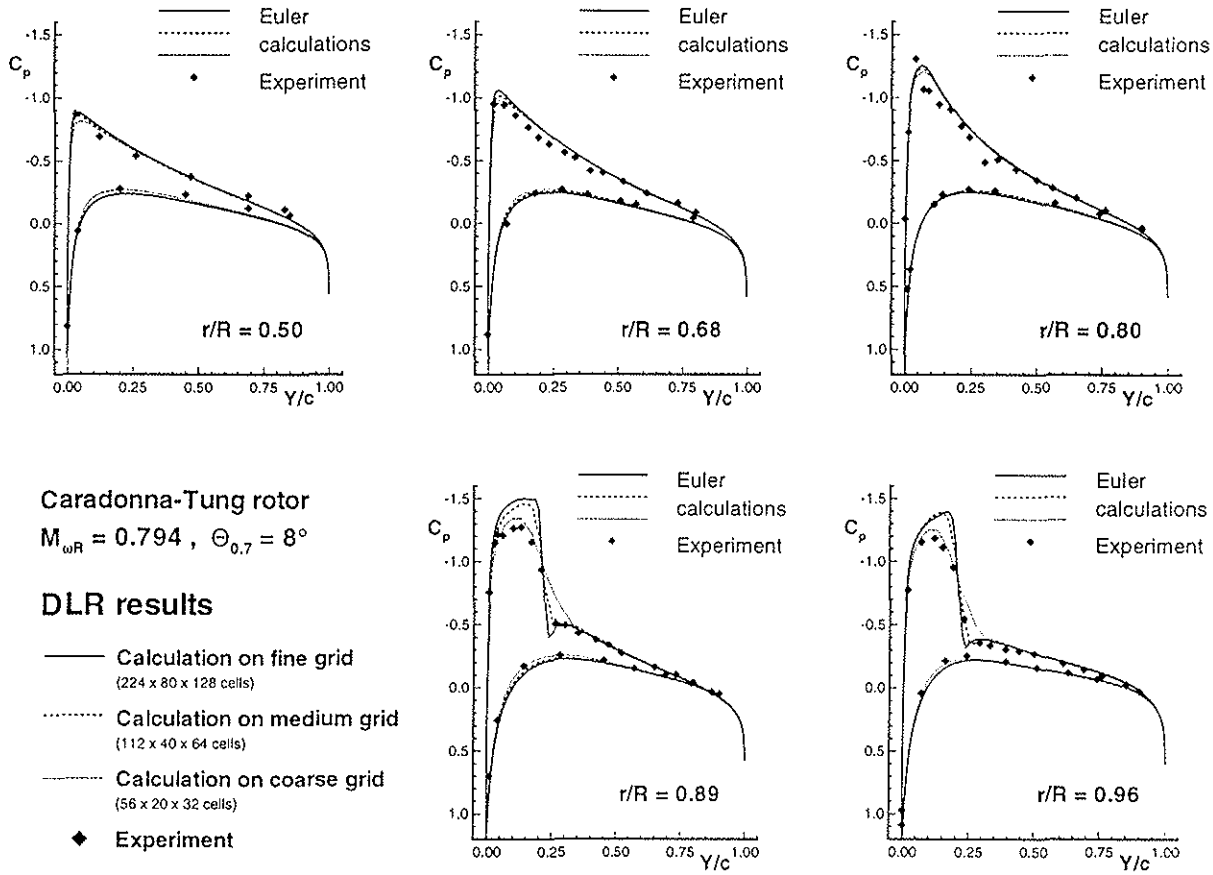

Figure 6 : Pressure distributions for 2-bladed Caradonna-Tung rotor: DLR results of grid refinement study

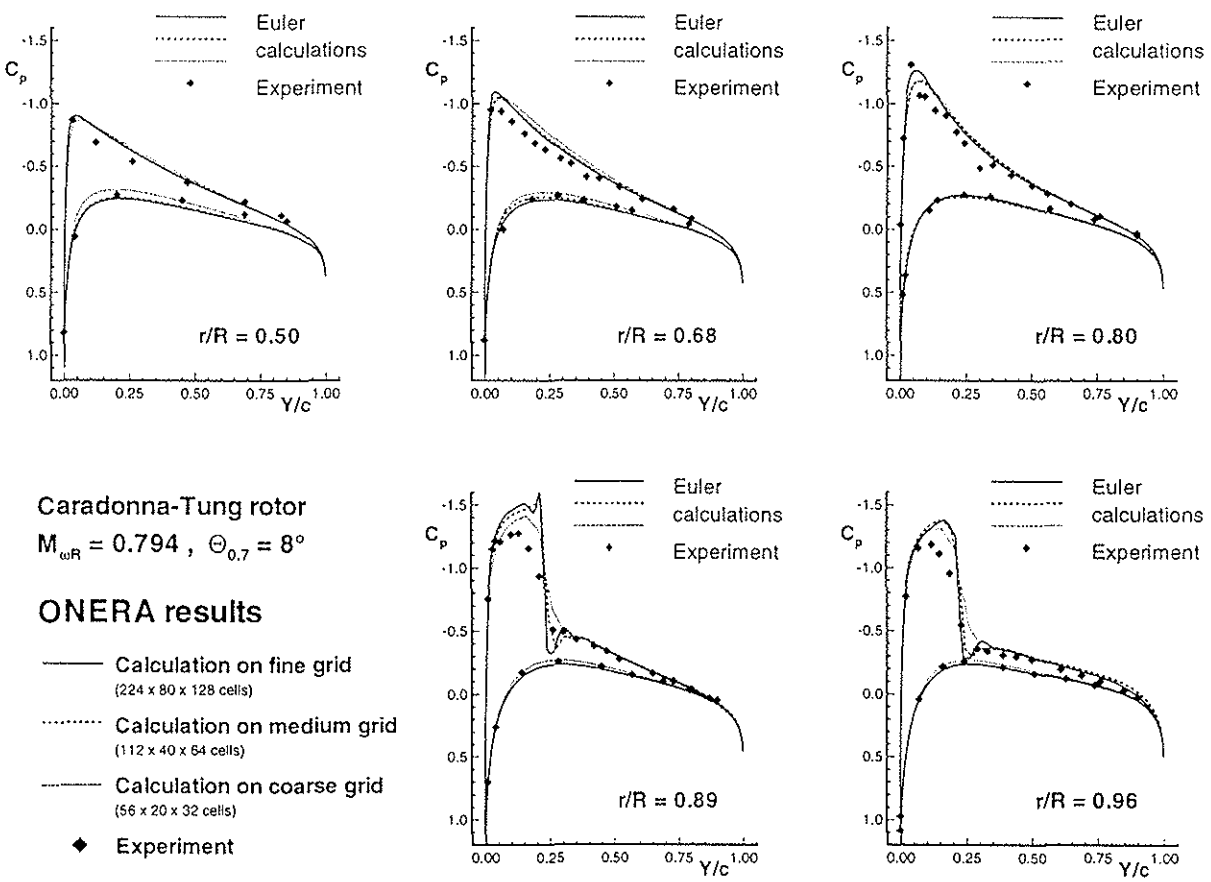

Figure 7 : Pressure distributions for 2-bladed Caradonna-Tung rotor: ONERA results of grid refinement study

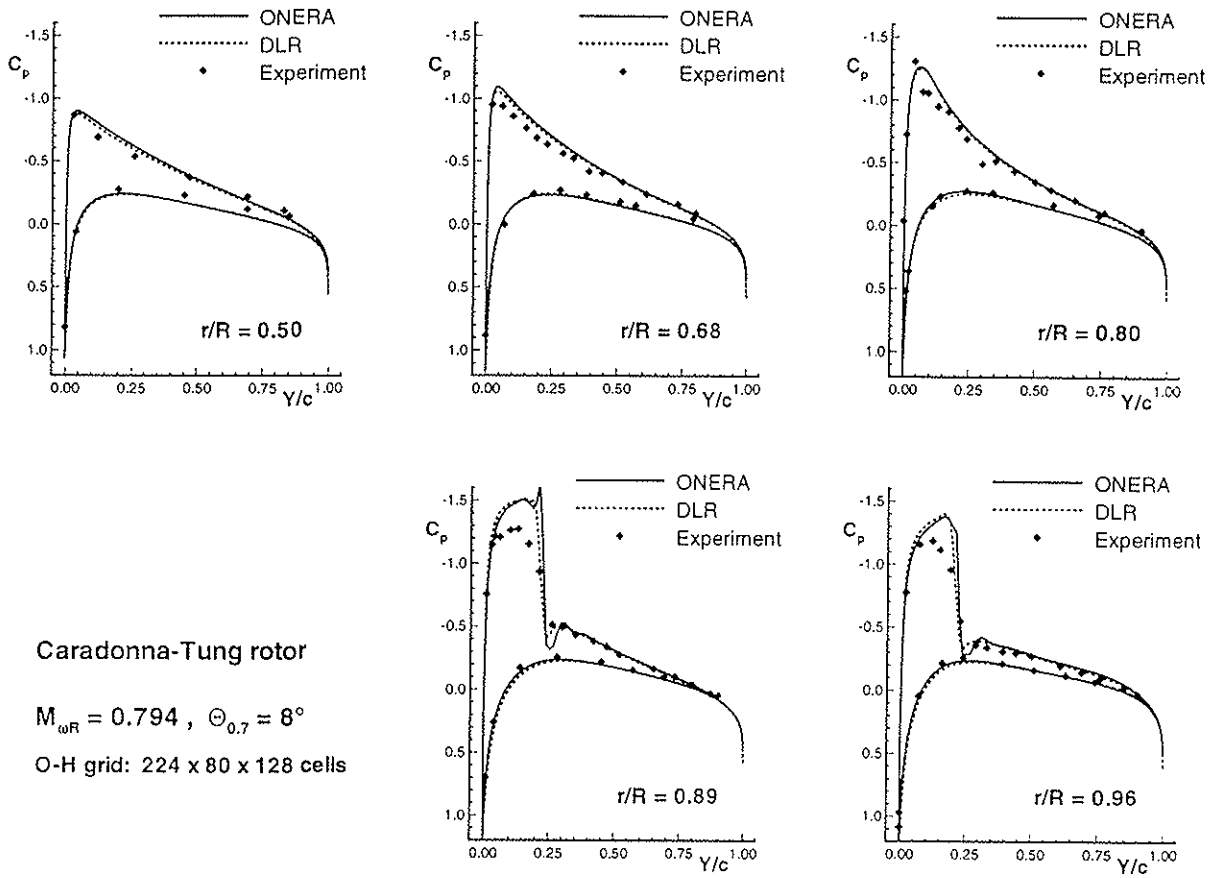

Figure 8 : Comparison of pressure distributions for 2-bladed Caradonna-Tung rotor: Euler calculations of DLR and ONERA on fine grid

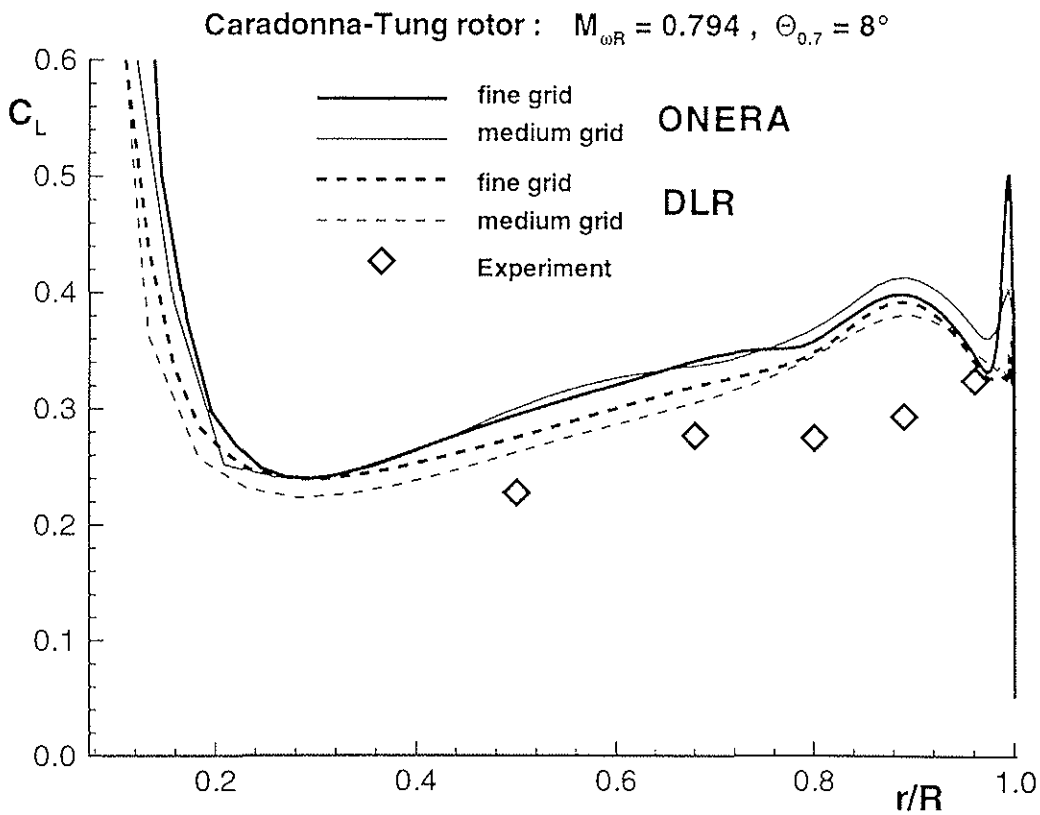

Figure 9 : Comparison of spanwise blade loadings for 2-bladed Caradonna-Tung rotor: Euler calculations of DLR and ONERA on fine and medium grids

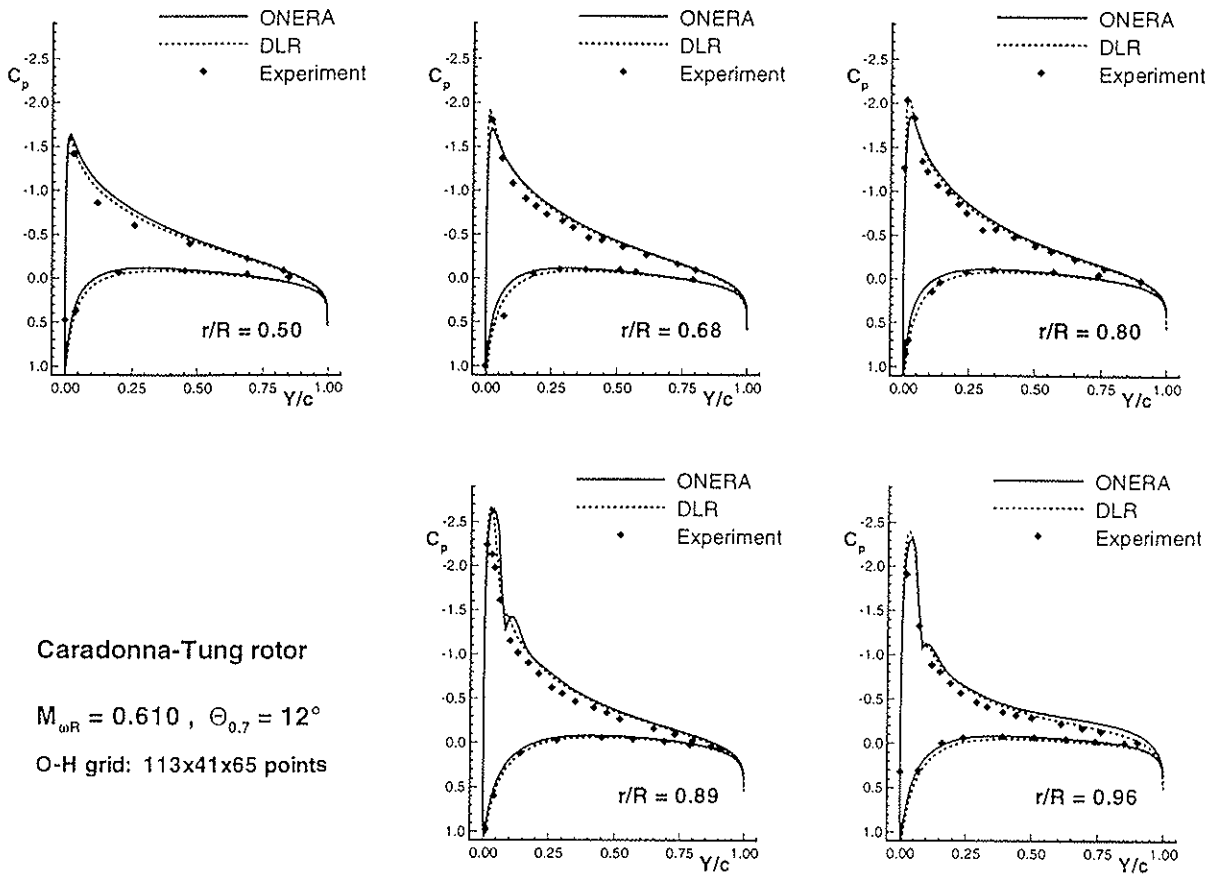

Figure 10 : Comparison of pressure distributions for 2-bladed Caradonna-Tung rotor: Euler calculations of DLR and ONERA

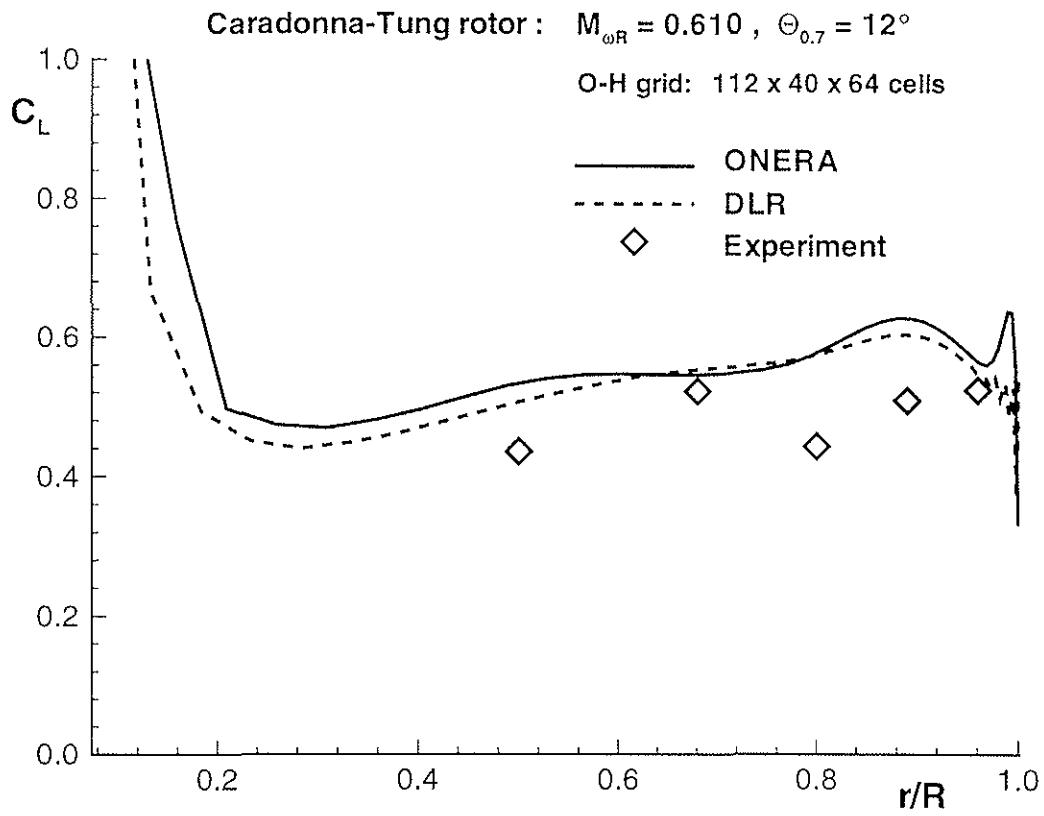

Figure 11 : Comparison of spanwise blade loadings for 2-bladed Caradonna-Tung rotor: Euler calculations of DLR and ONERA

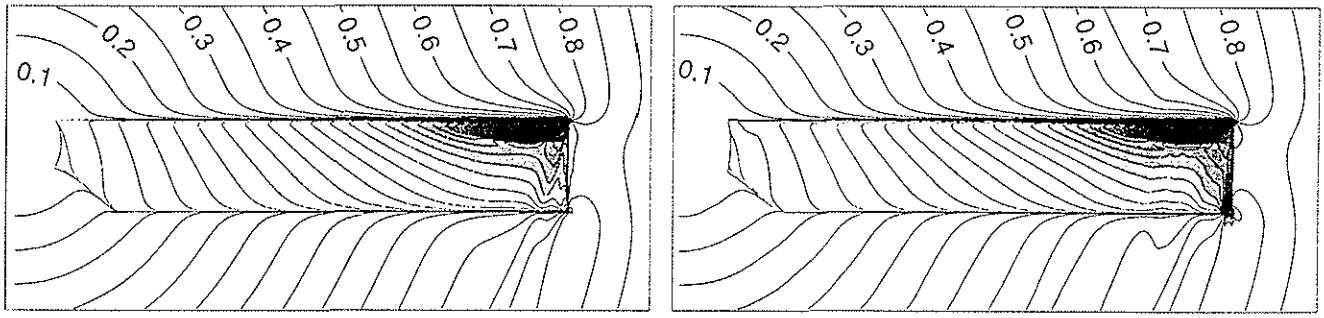

Figure 12 : Comparison of relative Mach number for Caradonna-Tung rotor: $M_{\omega R} = 0.794$, $\theta_{0.7} = 8°$, Euler calculations of DLR and ONERA on fine grid (224 x 80 x 128 cells)

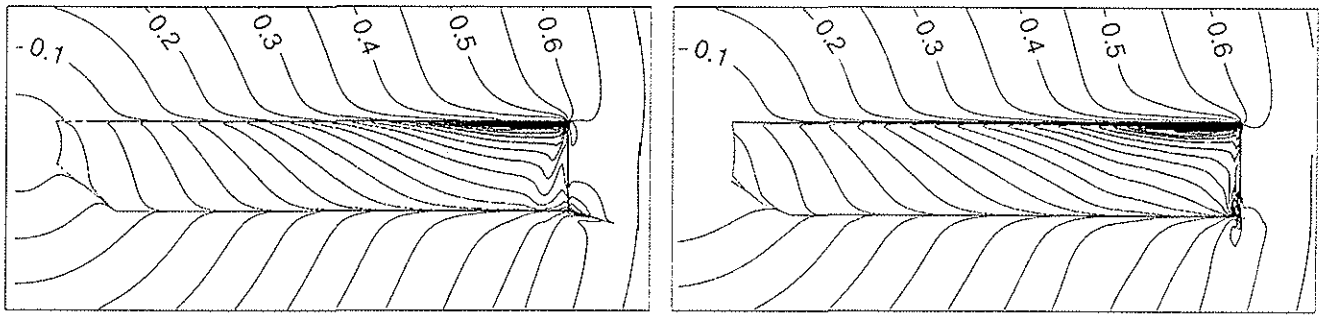

Figure 13 : Comparison of relative Mach number for Caradonna-Tung rotor: $M_{\omega R} = 0.610$, $\theta_{0.7} = 12°$

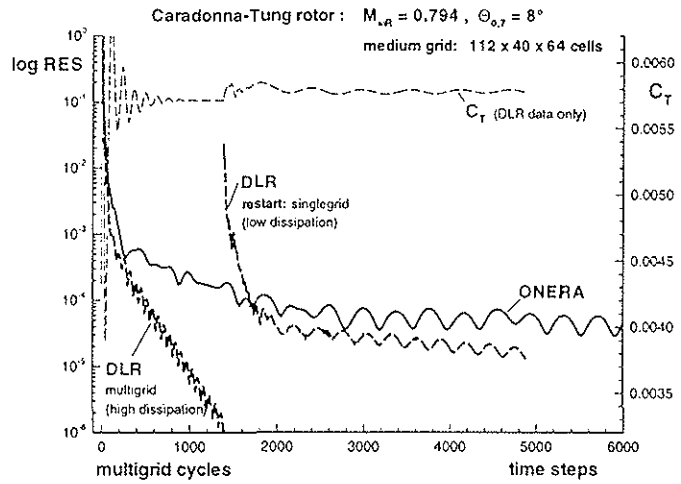

Figure 14 : Comparison of convergence behaviour of DLR and ONERA Euler codes calculating test case 1 (medium grid)

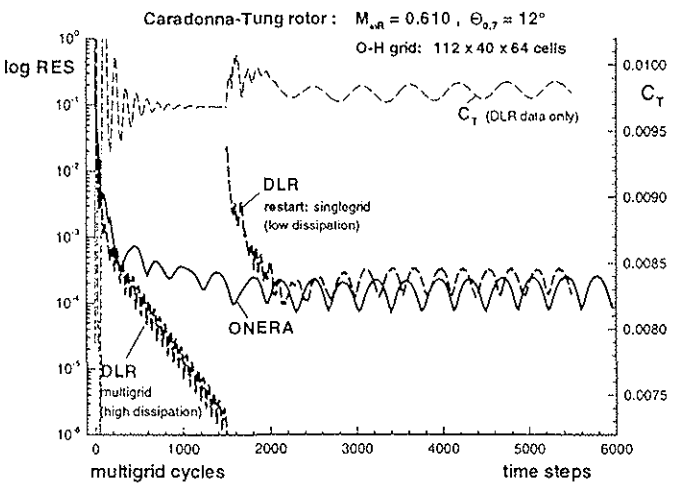

Figure 15 : Comparison of convergence behaviour of DLR and ONERA Euler codes calculating test case 2

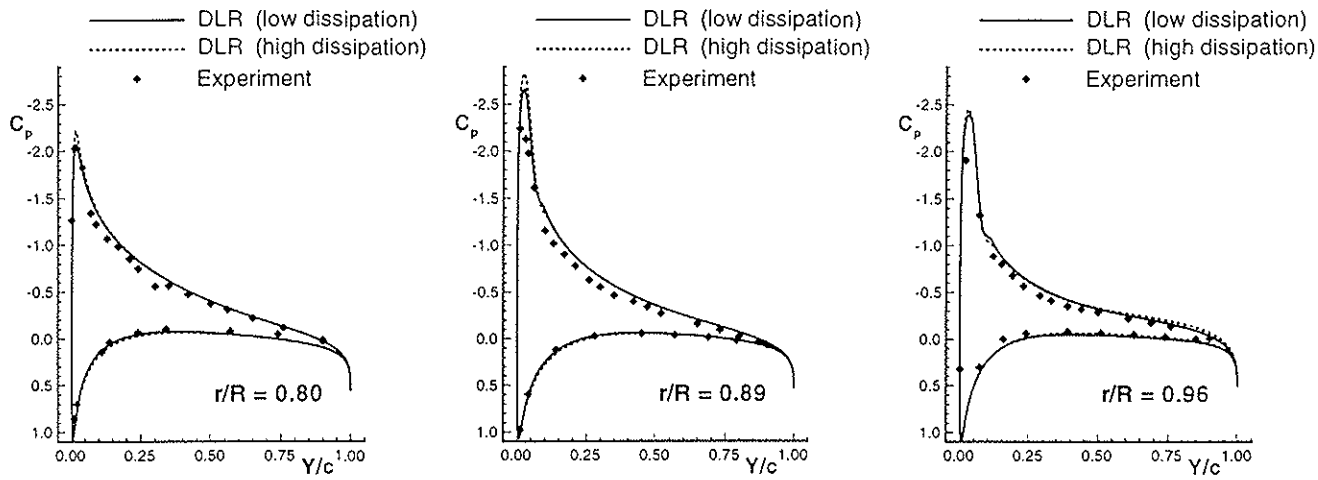

Figure 16 : Comparison of pressure distributions for Caradonna-Tung rotor: $M_{\omega R} = 0.610$, $\theta_{0.7} = 12°$, DLR Euler calculations using different values for artificial dissipation

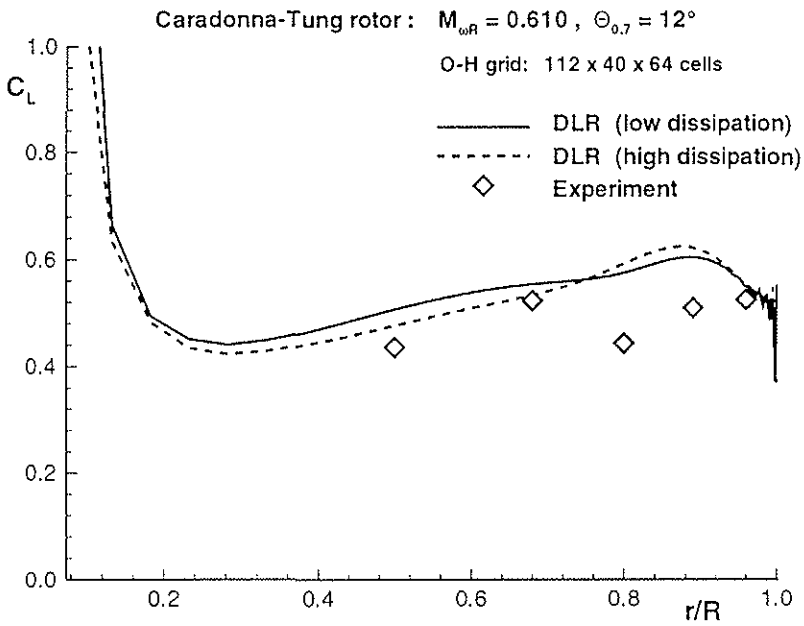

Figure 17 :
Comparison of spanwise blade loadings for 2-bladed Caradonna-Tung rotor:
DLR Euler calculations using different values for artificial dissipation

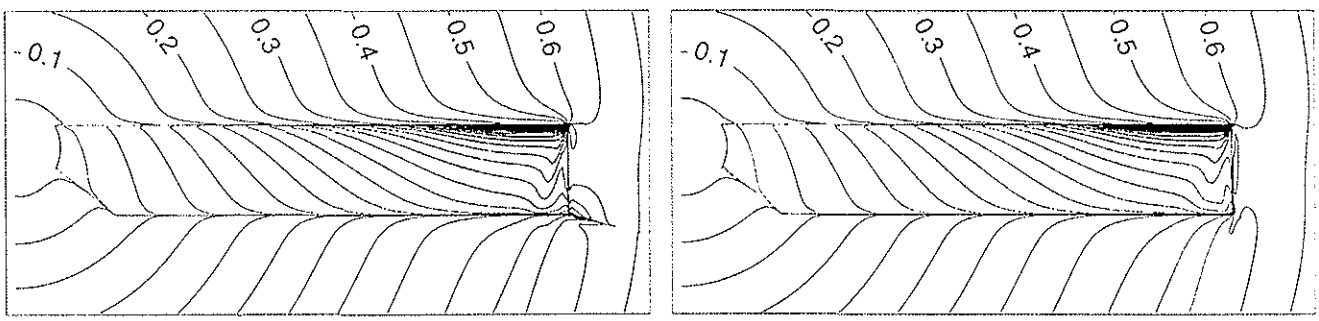

DLR calculation (low dissipation) DLR calculation (high dissipation)

Figure 18 : Comparison of relative Mach number for Caradonna-Tung rotor: $M_{\omega R} = 0.610$, $\theta_{0.7} = 12°$ DLR Euler calculations using different values for artificial dissipation

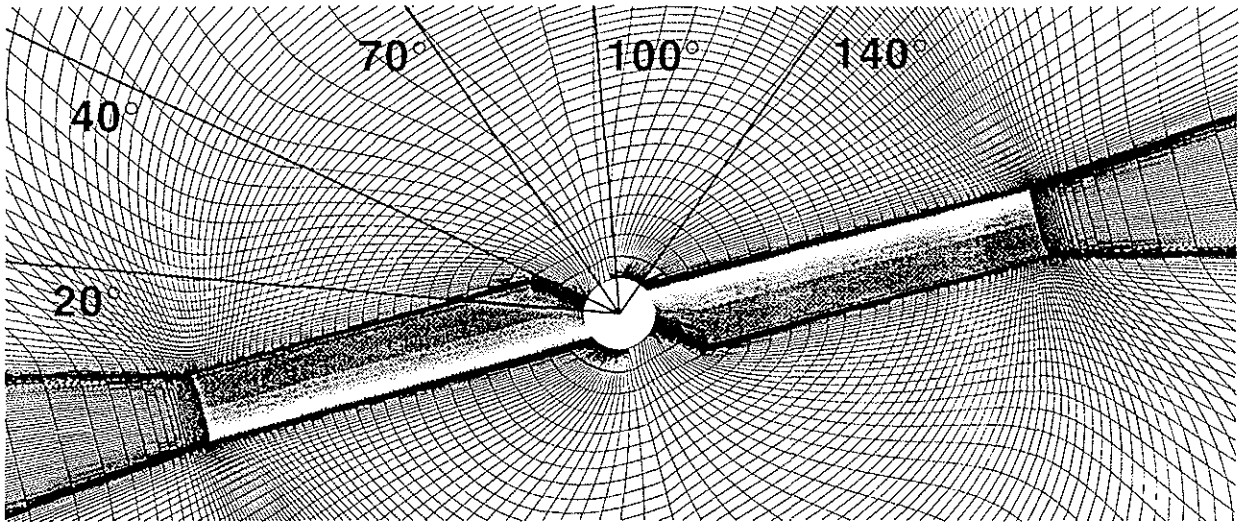

Figure 19 : Grid lines in the rotor disk for 2-bladed Caradonna-Tung rotor and position of radial slices presented in the following figures

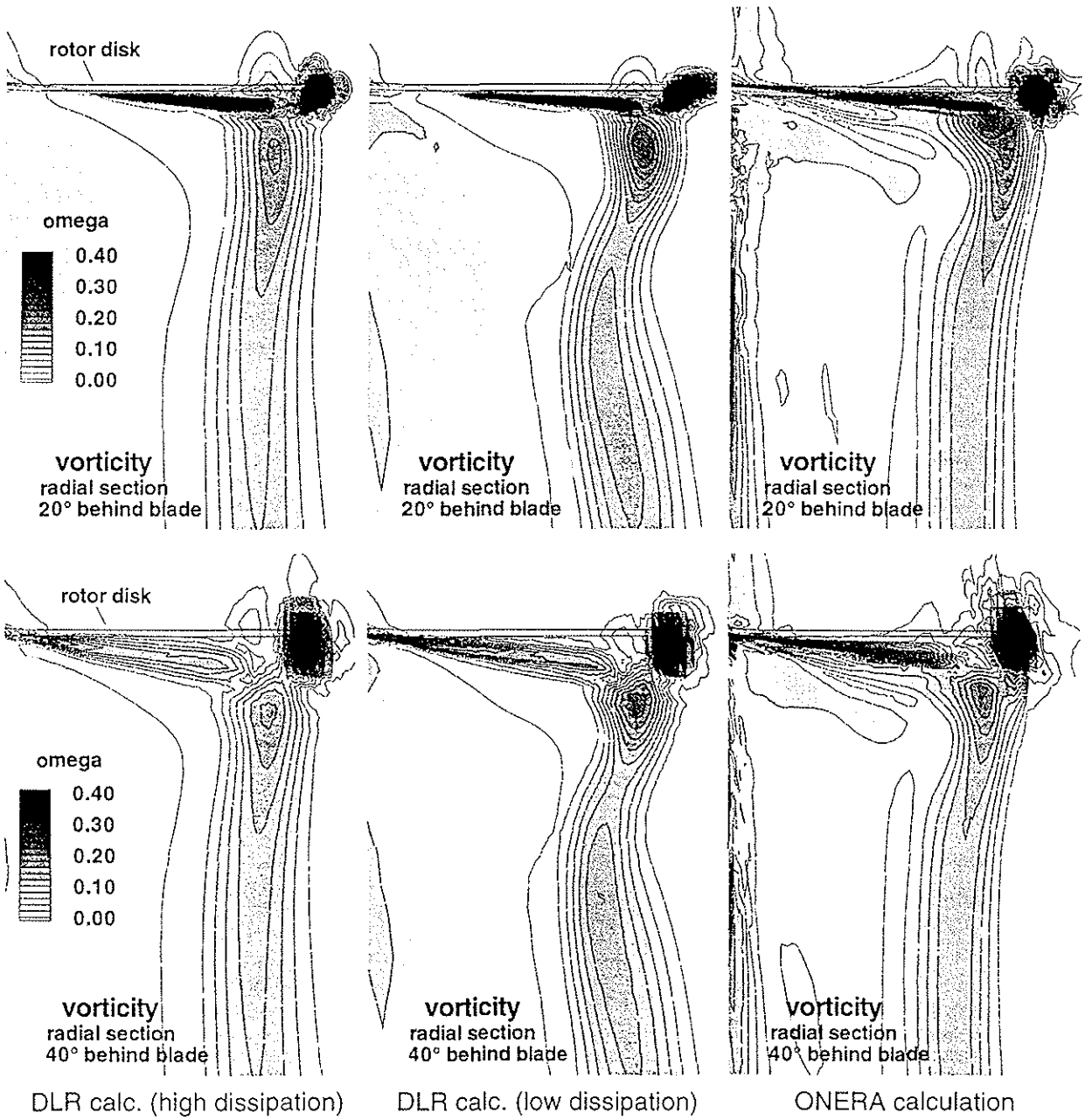

Figure 20 a, b : Vorticity contours of Caradonna-Tung rotor in hover at different radial sections, $M_{\omega R}$ = 0.610 , $\theta_{0.7}$ = 12° , grid size: 112 x 40 x 64 cells

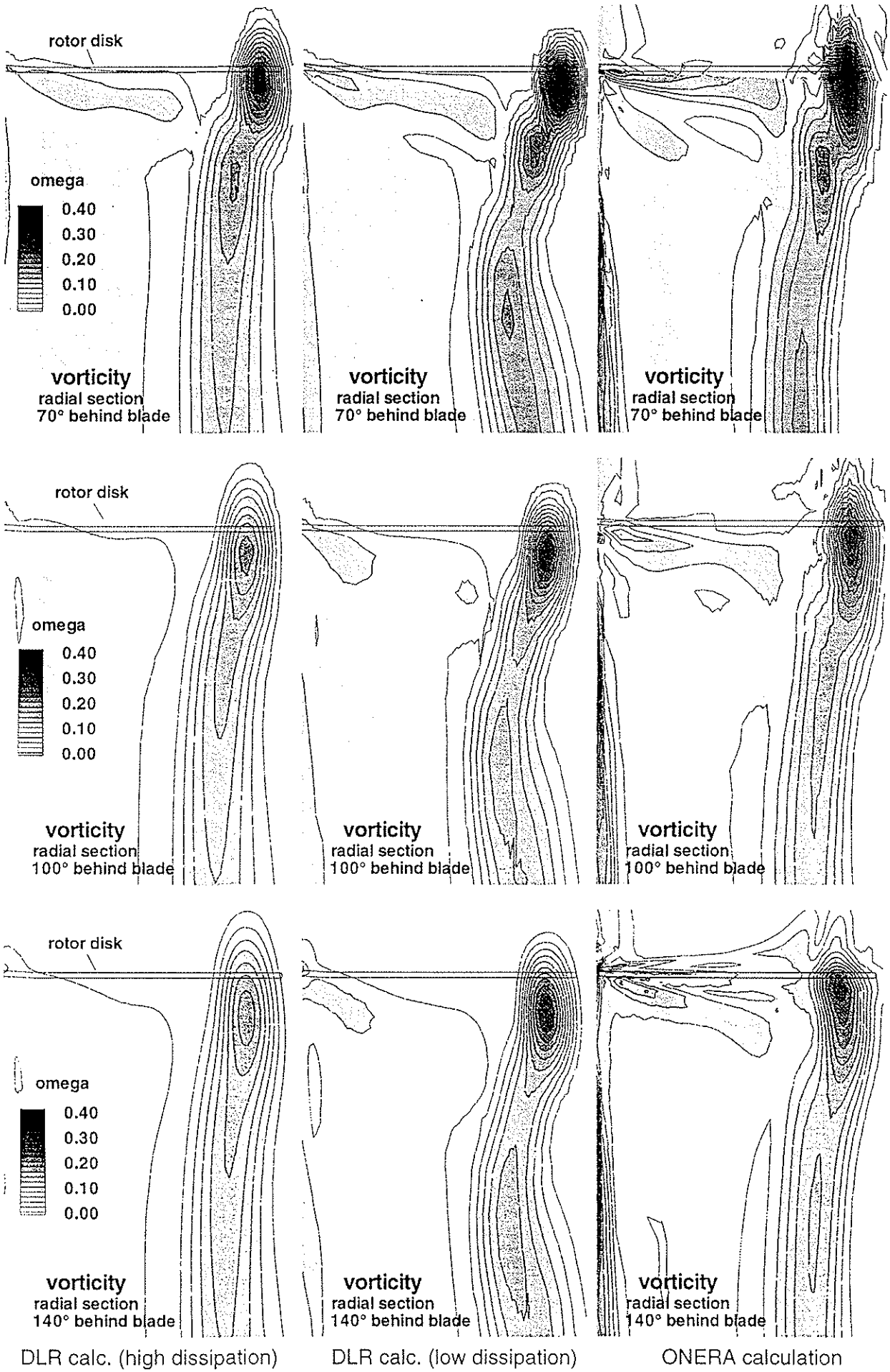

Figure 20 c - e : Vorticity contours of Caradonna-Tung rotor in hover at different radial sections, $M_{\omega R}$ = 0.610 , $\theta_{0.7}$ = 12° , grid size: 112 x 40 x 64 cells

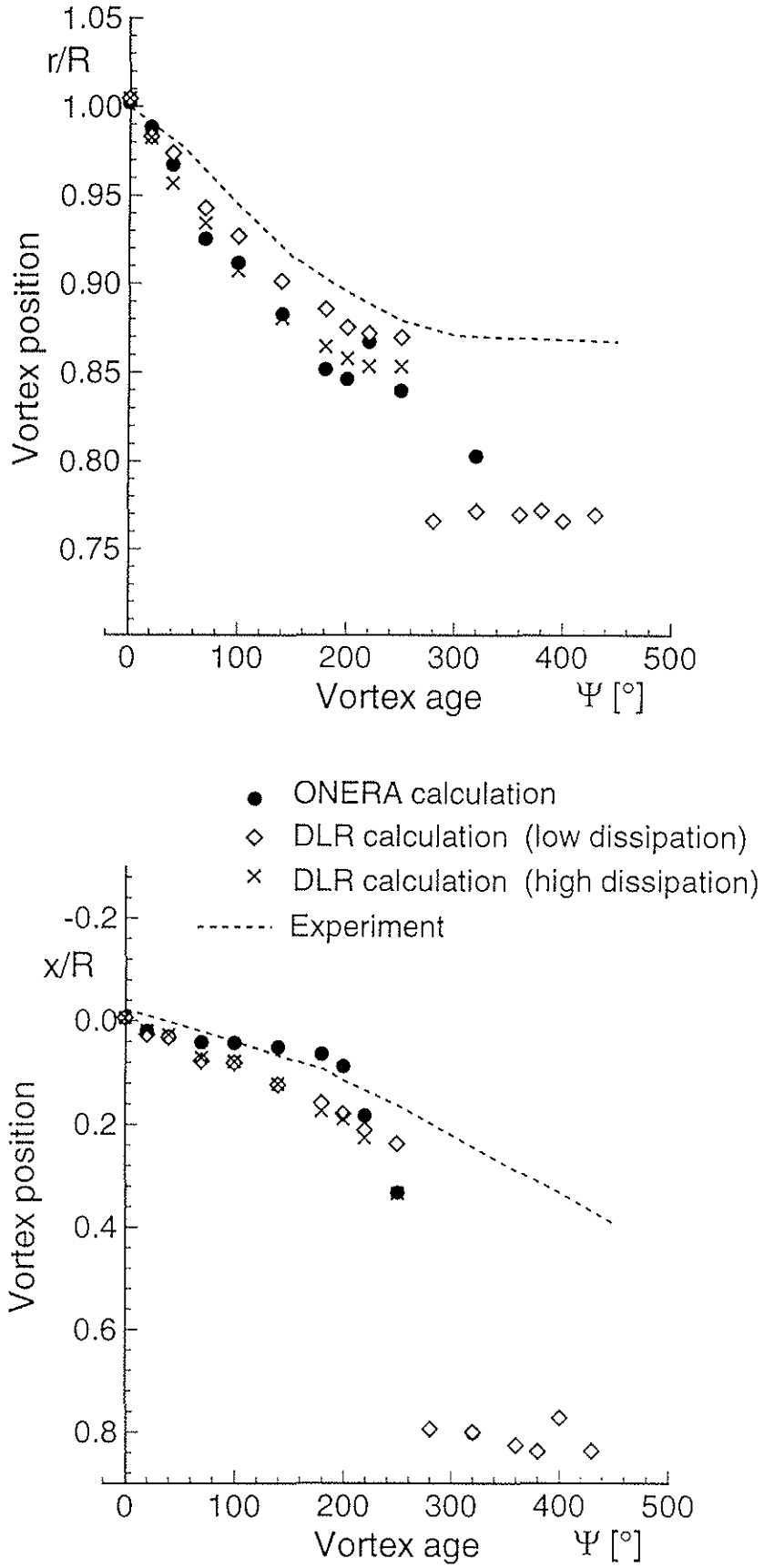

Figure 21 : Predicted and experimental vortex trajectories of Caradonna-Tung rotor in hover, $M_{\omega R} = 0.610$, $\theta_{0.7} = 12°$

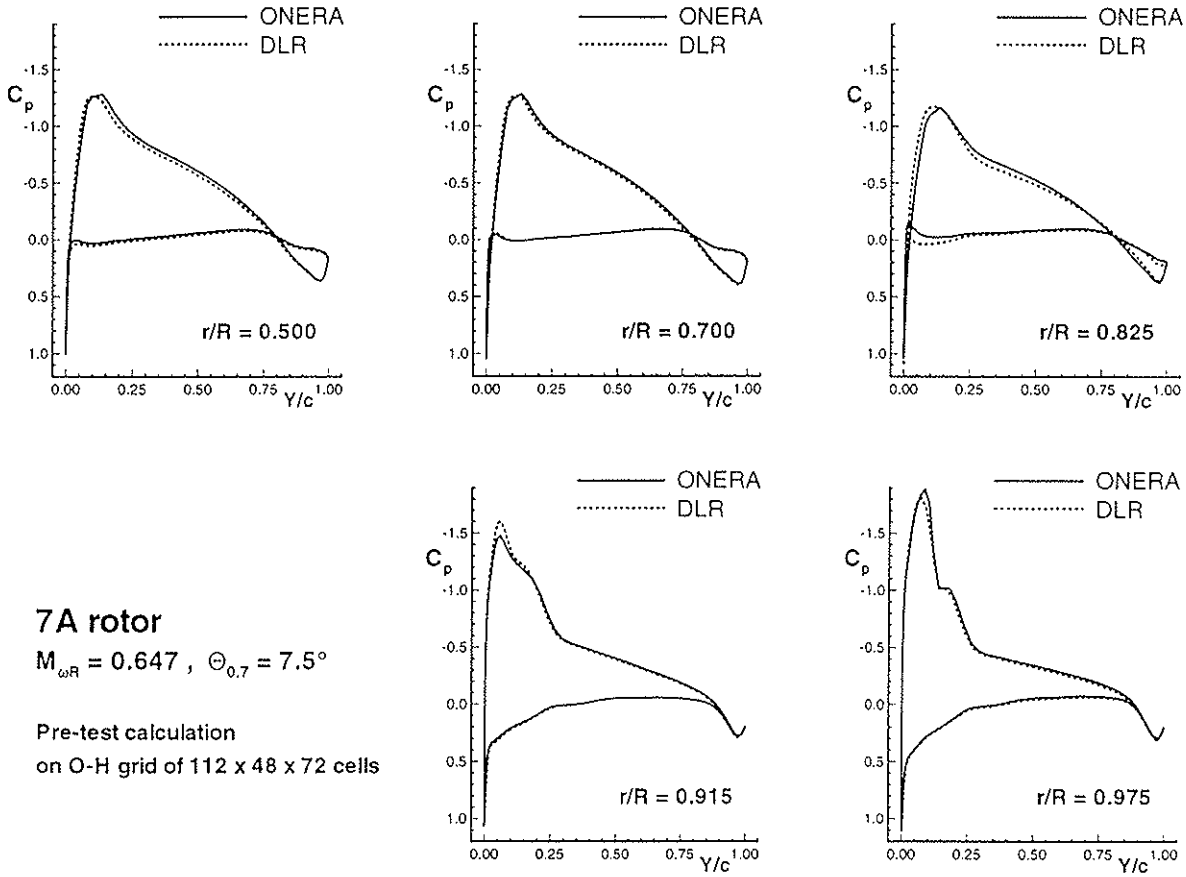

Figure 22 : Comparison of pressure distributions for 4-bladed HELISHAPE 7A rotor: Euler calculations of DLR and ONERA

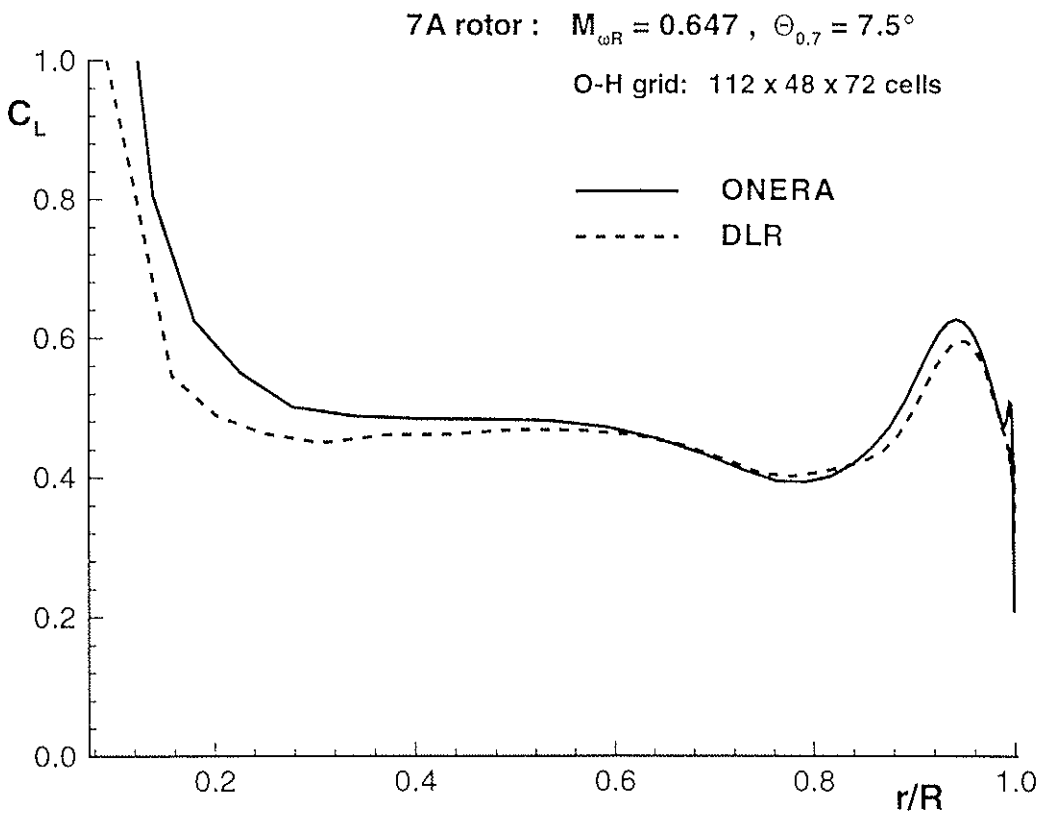

Figure 23 : Comparison of spanwise blade loadings for 4-bladed HELISHAPE 7A rotor: Euler calculations of DLR and ONERA